Human Glutathione-Dependent Formaldehyde Dehydrogenase. Structures of Apo, Binary, and Inhibitory Ternary Complexes†

Paresh C. Sanghani,‡ Howard Robinson,§ William F. Bosron,‡ and Thomas D. Hurley*,‡

Department of Biochemistry and Molecular Biology, Indiana University School of Medicine, Indianapolis, Indiana 46202, and Biology Department, Brookhaven National Laboratory Upton, New York 11973-5000

Received March 1, 2002; Revised Manuscript Received May 17, 2002

ABSTRACT: The human glutathione-dependent formaldehyde dehydrogenase is unique among the structurally studied members of the alcohol dehydrogenase family in that it follows a random bi bi kinetic mechanism. The structures of an apo form of the enzyme, a binary complex with substrate 12-hydroxydodecanoic acid, and a ternary complex with NAD^+ and the inhibitor dodecanoic acid were determined at 2.0, 2.3, and 2.3 Å resolution by X-ray crystallography using the anomalous diffraction signal of zinc. The structures of the enzyme and its binary complex with the primary alcohol substrate, 12-hydroxydodecanoic acid, and the previously reported binary complex with the coenzyme show that the binding of the first substrate (alcohol or coenzyme) causes only minor changes to the overall structure of the enzyme. This is consistent with the random mechanism of the enzyme where either of the substrates binds to the free enzyme. The catalytic-domain position in these structures is intermediate to the "closed" and "open" conformations observed in class I alcohol dehydrogenases. More importantly, two different tetrahedral coordination environments of the active site zinc are observed in these structures. In the apoenzyme, the active site zinc is coordinated to Cys44, His66 and Cys173, and a water molecule. In the inhibitor complex, the coordination environment involves Glu67 instead of the solvent water molecule. The coordination environment involving Glu67 as the fourth ligand likely represents an intermediate step during ligand exchange at the active site zinc. These observations provide new insight into metal-assisted catalysis and substrate binding in glutathione-dependent formaldehyde dehydrogenase.

Human glutathione-dependent formaldehyde dehydrogenase (FDH) is a class III alcohol dehydrogenase that, in addition to its activity toward primary alcohols and aldehydes, metabolizes biologically important glutathione adducts such as S-(hydroxymethyl)glutathione (HMGSH) and S-nitrosoglutathione (*1*−*3*). These latter two activities implicate FDH as an important component of two widespread cellular processes in living cells, viz. formaldehyde detoxification and the nitric oxide signaling (*3*, *4*). FDH shows poor catalytic efficiency for short-chain aliphatic alcohols such as ethanol and prefers long-chain alcohols such as ω-hydroxy fatty acids as substrates (*5*). The poor catalytic efficiency toward short chain alcohols can be enhanced by the addition of medium-chain fatty acids (*6*).

FDH is a highly conserved and ubiquitously expressed form of ADH that has been suggested to be progenitor of all isozymes within the family (*7*). In constrast to the more well-studied members of the ADH family, it obeys a random bi bi kinetic mechanism (*8*). Despite this kinetic difference, FDH has the same overall fold as other alcohol dehydrogenases and functions as a homodimer of two identical subunits with no evidence of cooperativity (*8*, *9*). Each subunit is made up of two domains: a coenzyme binding domain that forms much of the subunit interface and a catalytic domain located at the ends of the dimer. The active site is located in the cleft between the coenzyme-binding and catalytic domains. There are two zinc atoms in each of the subunits. One zinc atom is in the active site and functions as a Lewis acid to activate alcohols during catalysis. The other zinc is coordinated to four cysteines and apparently plays a structural role.

The previously reported structure of FDH in a binary complex with its coenzyme had notable structural differences with the published structures for horse and human ADHs (*9*). In the FDH·NAD(H) binary complex, the relative position of the catalytic and coenzyme-binding domains was intermediate between the fully "open" and fully "closed" domain conformations described for horse alcohol dehydrogenase. Furthermore, the catalytic zinc coordination geometry differed from the well-characterized tetrahedral coordination found in all other ADH isoenzymes whose structure was

† This work is supported by Grants R37-AA07117, R29 AA10399, and P50 AA07611. P.C.S. is supported by grant F32 AA05568.

* Corresponding author. Address: Department of Biochemistry and Molecular Biology, Indiana University School of Medicine, 635 Barnhill Dr., Indianapolis, IN 46202. Tel. 317-274-2008. Fax: 317-274-4686. Email: thurley@iupui.edu.

‡ Indiana University.

§ Brookhaven National Laboratory.

[1] Abbreviations: 12-HDDA, 12-hydroxydodecanoic acid; HMGSH, S−(hydroxymethyl)glutathione, ADH, alcohol dehydrogenase; FDH, human glutathione-dependent formaldehyde dehydrogenase.

[2] The structure factors and atomic coordinates of the apoenzyme, FDH·12-HDDA binary complex, and FDH·NAD^+·Dodecanoic acid ternary complexes have been deposited in the Brookhaven Protein Data Bank under ID codes 1M6H, 1M6W, and 1MAO, respectively.

10.1021/bi0257639 CCC: $22.00
Published on Web 08/27/2002

known. In the FDH·NADH binary complex, the zinc exhibited a pentacoordinate environment in one of the active sites, with Glu67 positioned as a fifth ligand in addition to the standard ligands Cys44, Cys174, and His66 and a water molecule. The present study describes the structures of apo, binary alcohol, and inhibitor ternary FDH complexes that further explore its random substrate binding mechanism and active site zinc coordination structures.

MATERIALS AND METHODS

All chemicals used in this study were obtained from Sigma Chemical Co. Recombinant human FDH was expressed in *E. coli* and purified according to published procedures (*8*) with the following modification to obtain coenzyme-free enzyme. The enzyme was eluted with 2M NaCl from the Mimetic Blue 2 column (ProMetic Biosciences, Inc.) instead of using a NAD^+ gradient. The purified enzyme was stored at −20 °C in 50% glycerol (v/v), and glycerol was removed prior to crystal growth by gel filtration.

Crystal growth. Crystals of the apoenzyme were grown using the sitting-drop vapor-diffusion method at 4 °C from a 15−20 mg/mL enzyme solution equilibrated with 0.1 M potassium phosphate buffer pH 6.9−7.1, 100 μM $ZnSO_4$, 1 mM DTT, and 12−15% PEG8000. Crystals grew as rectangular rods after 8 days and reached full size in about 2 weeks. Crystals of the FDH·12-HDDA (12-hydroxydodecanoic acid) binary complex were obtained by soaking the apoenzyme crystals with fresh crystallization buffer containing 2 mM 12-HDDA for 3 days. Crystals of the FDH·NAD^+·dodecanoic acid complex were obtained by initially soaking the crystals of apoenzyme with crystallization buffer containing 2 mM dodecanoic acid for 2 days. Following this, the crystals were then transferred to freshly prepared crystallization buffer containing 2 mM dodecanoic acid and 2.5 mM NAD^+ for 3 h. For data collection, a quick two-step soaking procedure was used to introduce 21% (v/v) PEG400 into the standard crystallization buffer before flash-freezing the crystals at −165 °C in a gaseous nitrogen stream. Initial analysis of the diffraction using an Raxis IIc image plate detector and a Rigaku RU 200HB rotating anode generator revealed cell dimensions of 79 × 79 × 310 Å and a spacegroup of $P4_32_12$. The crystals were stored in liquid nitrogen following this preliminary analysis and shipped to the NSLS/Brookhaven National laboratory for high-resolution data collection.

Data collection and structure solution. A three-wavelength Multiwavelength Anomalous Dispersion (MAD) data set was collected for each different enzyme form using the Zn-absorption edge on the X12B beamline at NSLS/Brookhaven National laboratories. The highly redundant data (greater than 13 observations per unique reflection) were integrated and scaled with the program HKL2000 in space group $P4_32_12$ (*10*). The phases were solved using the program SOLVE (*11*) and improved using the program RESOLVE (*12*). After placing the FDH·NAD(H) binary complex model in the MAD map, the structure was manually fitted and then refined using the program CNS (*13*). In the initial stages of refinement of all structures, noncrystallographic symmetry restraints of 100 kcal/mol were applied to the main chain atoms in the dimer and 10 kcal/mol for the side chain atoms. These restraints were removed in the later cycles of refinement. All models were refined against all available data by applying a bulk-solvent correction to the low-resolution data and individual restrained isotropic temperature factors for all the atoms. The nonbonded ionic radius of active site zinc was reduced from 1.57 to 0.75 Å in the ion parameter file of CNS to maintain ligand geometry observed in high-resolution structures of horse liver EE isoenzyme (*14*, *15*). Visual inspection of the resulting models during refinement was carried out using the program O (*16*). Solvent molecules were added as indicated by the presence of strong electron density peaks in F_o-F_c maps within hydrogen-bonding distance to appropriate protein atoms. The topology and parameter files for 12-HDDA and dodecanoic acid were made using the XPLO2D program (*17*).

RESULTS

Structure solution and analysis. Structures of the apo-FDH, the FDH·12-HDDA binary complex, and the FDH·NAD^+·dodecanoic acid ternary complex were determined at 2.0, 2.3, and 2.3 Å resolution, respectively, by Multiwavelength Anomalous Dispersion (MAD) using the absorption edge for the four covalently bound zinc atoms within the ADH dimer, which is comprised of a total of 746 amino acids. Despite the very weak anomalous signal from the four zinc ions (signal equivalent to ∼16 electrons), the structures were successfully phased without the aid of the preexisting model (Table 1). Following the solution and improvement of the phases using the programs SOLVE and RESOLVE, the previously obtained FDH·NAD(H) binary complex structure (*9*) was adjusted to fit the MAD map. The crystal packing in these three new structures were nearly identical and a functional dimer formed the asymmetric unit. The data collection and refinement statistics are found in Tables 1 and 2.

The three models of all the structures are of good quality (Table 2), with no nonglycine residues in the disallowed regions of their respective Ramchandran plots (not shown). All three structures have two potassium and two phosphate buffer ions bound to the protein surface. The apoenzyme and the FDH·12-HDDA binary complex models have an additional buffer phosphate ion bound within their coenzyme-binding site.

There are differences in the lattice contacts near the active sites of individual subunits in the asymmetric unit. Residues near the B-subunit active site make two additional crystal contacts than those near the A-subunit active site. These additional crystal contacts are close to the loops comprised of residues 47−58, 361−367, and 291−298. Fewer crystal contacts also make the active site in the A-subunit more accessible than that in the B-subunit. The catalytic domain of the A-subunit has higher overall temperature factor than the catalytic domain in the B-subunit, reflecting this environment.

Overall Structural changes in FDH complexes. Very small differences are observed in the catalytic domain conformation of the three FDH complexes reported here (Figure 1). The position of the catalytic domain in these complexes is similar to the one observed in the previously reported FDH·NAD(H) binary complex (*9*) and intermediate between the "open" and "closed" positions observed in the horse liver ADH (*18*−*20*). Since the crystal packing contacts in our structures and the previously reported FDH·NAD(H) binary complex differ,

Table 1: Data Collection Statistics

	MAD inflection	MAD peak	MAD remote	native
		Apoenzyme		
wavelength (Å)	1.2833	1.2823	1.2770	0.9790
observations (total/unique)	885,886/55,055	754,323/55,165	772,477/55,706	508,528/64,501
completeness (%)[a]	94.7 (83.6)	94.7 (83.8)	94.4 (83.7)	96.1 (87.6)
R_{merge}[a,b]	6.5 (31.7)	6.6 (31.6)	6.8 (34.5)	6.9 (43.8)
$I/\sigma I$[a]	40.1 (6.9)	34.1 (5.9)	34.1 (5.7)	24.2 (4.3)
resolution (Å)	20−2.1	20−2.1	20−2.1	30−2.0
unit cell (Å)			79.1, 79.1, 311	78.6, 78.6, 310
SOLVE/RESOLVE FOM[c]			0.63 (20−2.2)	
		FDH:12-HDDA Binary Complex		
wavelength (Å)	1.2837	1.2827	1.2667	
observations (total/unique)	972,317/44,036	1,037,848/44,113	1,039,956/43,971	
completeness (%)[a]	98.2 (86.4)	98.3(86.9)	98.9 (90.6)	
R_{merge}[a,b]	9.5 (36.5)	9.8(36.5)	9.2 (28.8)	
$I/\sigma I$[a]	30.4 (5.1)	30.7(5.4)	37.4 (7.5)	
resolution (Å)	20−2.3	20−2.3	20−2.3	
unit cell (Å)			78.6, 78.6, 309	
SOLVE/RESOLVE FOM[c]			0.64 (19.8−2.5)	
		FDH:NAD^+:Dodecanoic Acid Ternary Complex		
wavelength (Å)	1.2836	1.2835	1.2652	
observations (total/unique)	923,229/50,418	862,994/50,362	912,188/44,569	
completeness (%)[a]	99(93.8)	99(93.2)	99.8(98.4)	
R_{merge}[a,b]	9.9(32.6)	10.2(36.1)	10(32)	
$I/\sigma I$[a]	30.9(5.6)	28.3(4.8)	33.6(9.0)	
resolution (å)	20−2.2	20−2.2	20−2.3	
unit cell (å)			78.7, 78.7, 311	
SOLVE/RESOLVE FOM[c]			0.66 (19.8−2.5)	

[a] Data from the highest resolution shell is shown in parentheses. [b] $R_{merge} = \sum_{hkl}|I_i - I_n|/\sum I_n$, where I_i is an observed intensity and I_n is the average of the observed equivalents. [c] Figure of Merit for all the reflections to the indicated resolution.

Table 2: Refinement Statistics

	apoenzyme (native)	FDH:12-HDDA binary complex (remote)	FDH:NAD^+:dodecanoic acid ternary complex (remote)
amino acid residues	746	746	746
solvent molecules	901	672	555
$R_{work}(R_{free})$	18.5 (21.8)	19.2 (22.6)	19.3 (22.4)
average *B*-factor	23.30	25.35	29.50
rmsd bonds (Å)	0.005	0.005	0.006
rmsd angles (deg)	1.5	1.41	1.49

it is probable that the intermediate or "semi-open" catalytic domain conformation in FDH is independent of crystal packing interactions.

There are three notable localized movements involving residues 47−58, 291−298, and 361−367 in the three FDH complexes reported here. These residues line the active site and show movement only in the A-subunit, where they are not constrained by lattice contacts. The loop comprised of residues 291−297 is drawn inward by the binding of 12-HDDA in the FDH·12-HDDA binary complex (Figure 1). However, the loop is clearly mobile and moves back to its original position in the FDH·NAD^+·dodecanoic acid ternary complex (Figure 1). Residues 47−58 are also drawn toward 12-HDDA in the FDH·12-HDDA binary complex (Figure 1), although not to the extent as residues 291−298. Residues 361−367, which are drawn over the mouth of active site in the apoenzyme, retract in the binary and ternary complexes to open up the active site further.

Interactions in the substrate-binding site of FDH. Although 12-HDDA and dodecanoic acid have similar structures, there are differences in their interactions in the FDH active site. These differences appear to be influenced by the presence of the coenzyme in the FDH·NAD^+·dodecanoic acid ternary complex. In the absence of coenzyme, 12-HDDA adopts multiple conformations in the active site, as judged from its discontinuous electron density as well as its relatively high-temperature factors. Although the electron density for 12-HDDA in the original MAD map was discontinuous, it was strong at the carboxyl end of the molecule (Figure 2). This suggested that the carboxyl group of 12-HDDA was a major point of contact for 12-HDDA in the FDH active site. A simulated-annealing F_o-F_c omit map showed continuous positive electron density for the carboxyl group of 12-HDDA and the next 8−10 carbon atoms, beyond which the density decreased. Contouring the electron density at a lower level shows continuous density up to the active site zinc. Although occupancy assignments at the resolution of these structures are not entirely reliable, our analysis suggests that the hydroxyl group of 12-HDDA coordinates to the active site zinc >50% of the time, with a water molecule occupying the zinc site the remainder of the time. Accordingly, we have modeled the complex to show the predominant binding mode of the substrate (Figure 2). The carboxyl group of 12-HDDA interacts with Gln111, Arg114, and Lys283* (*from the other subunit). Residues Gln111 and Lys283 have identical conformations in each of the three FDH complexes reported here. Arg114 has been implicated in the binding of HMGSH as well as ω-hydroxyacids (*21*). The side chain of Arg114

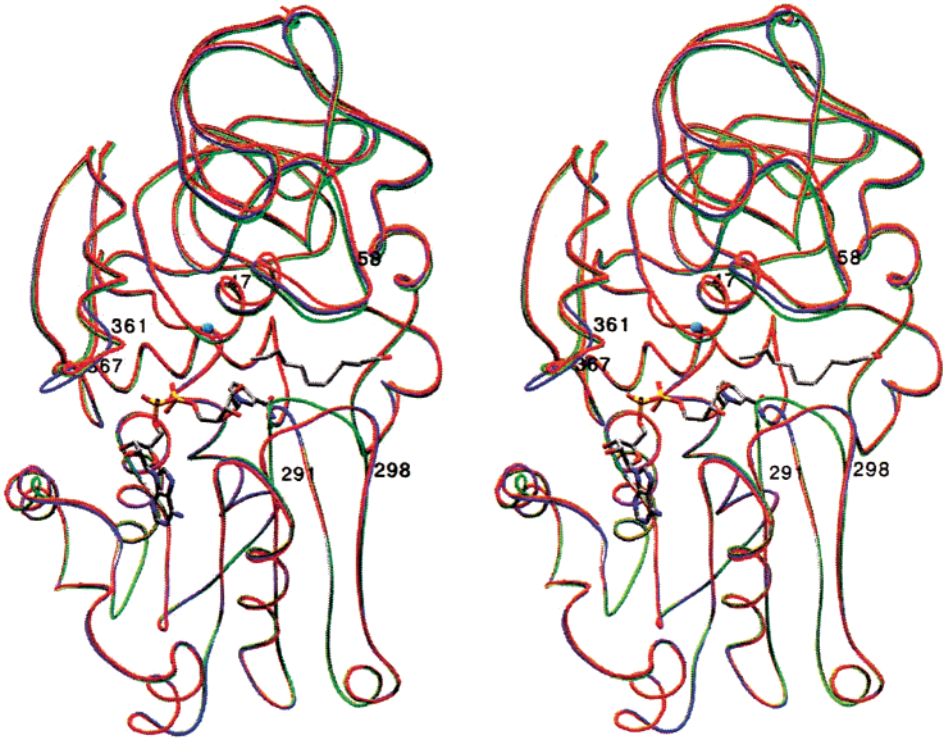

FIGURE 1: Structural differences between FDH complexes with different bound ligands. Residues 180−289 and 301−320 of the coenzyme-binding domain in the A-subunit of FDH·12-HDDA binary complex (green) and FDH·NAD^+·dodecanoic acid ternary complex (red) were aligned on to the corresponding residues in the apoenzyme (blue) using the LSQKAB routine of the CCP4 program package. Residues 47−58, 291−298, and 361−367, lining the active site are marked. The catalytic zinc, NAD^+, and dodecanoic acid are shown. All the figures were generated using Swiss-Pdb Viewer (*31*) and rendered using POV−Ray for windows (downloaded from www.povray.org).

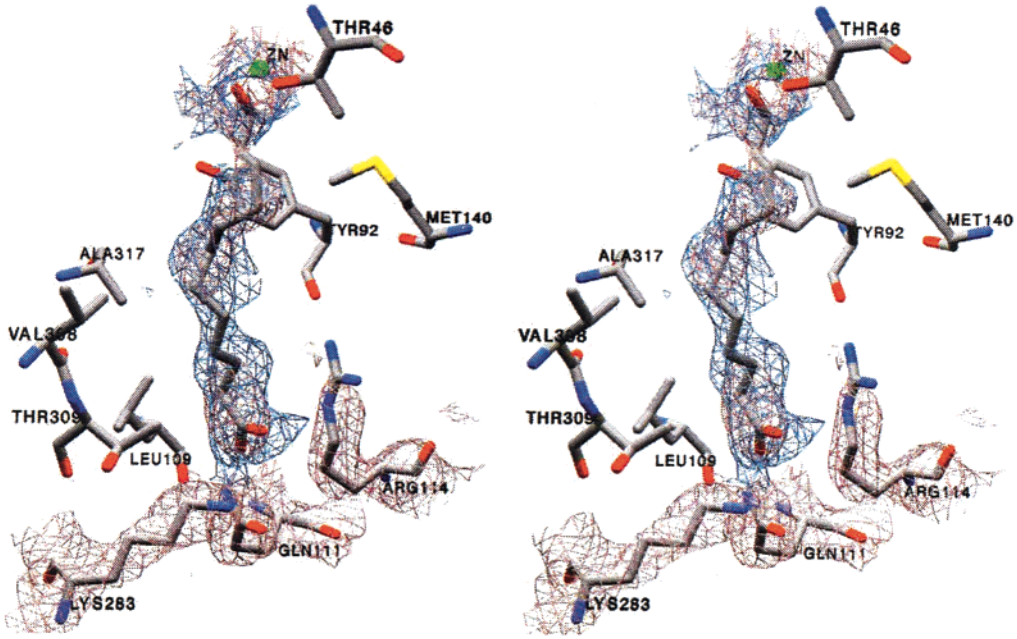

FIGURE 2: Interactions between 12-HDDA and FDH in the binary complex. The residues within 4 Å of the 12-HDDA molecule in the A-subunit of the FDH·12-HDDA binary complex are shown. The electron density contoured at one standard deviation of the original MAD map for 12-HDDA, Gln111, Arg114, Lys283, and active site zinc is displayed in light brown color. The F_o-F_c omit map density for the substrate contoured at 2.5 standard deviations is also shown in blue.

exhibits two conformations in three FDH structures reported here. Examples of these two conformations are illustrated in the binary and ternary complexes where Arg114 interacts differently with the bound 12-HDDA and dodecanoic acid molecules (Figures 2 and 3). In the active site of the A-subunit, the long hydrophobic chain of 12-HDDA makes van der Waals contacts with Tyr92, Leu109, Met140, Gly292, and Ala317 from the A-subunit and Val308 and Thr309 from the B-subunit. In the B-subunit of the binary complex, the van der Waals interactions of 12-HDDA involve Val293, Ile93, Tyr92, Ala317, and Val308 from the A-subunit.

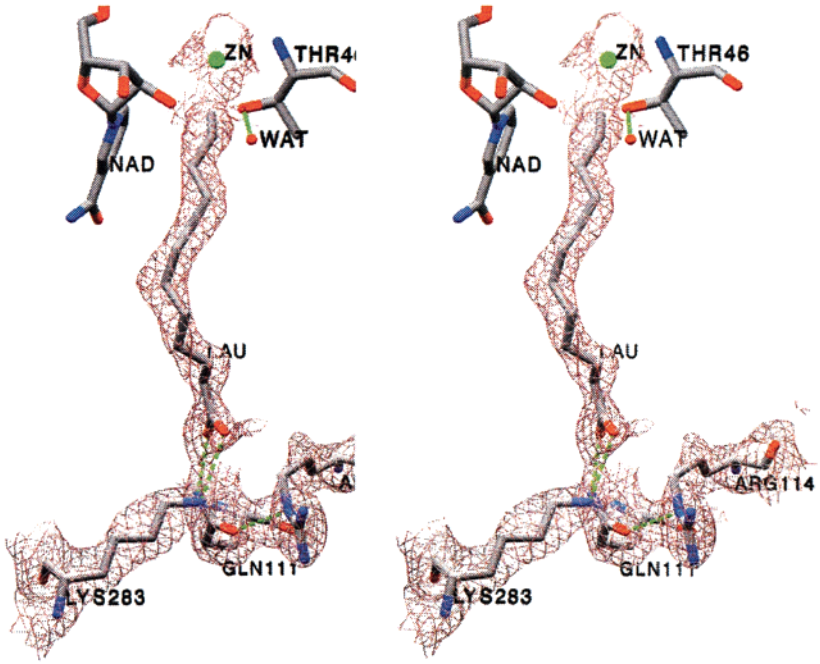

FIGURE 3: Interactions of dodecanoic acid (LAU) in the FDH·NAD^+·dodecanoic acid ternary complex. The final $2F_o-F_c$ map (contoured at one standard deviation) showing electron density for dodecanoic acid in the A-subunit of the ternary complex.

Dodecanoic acid is significantly more ordered in the active site of the inhibitor ternary complex (Figure 3) compared with the 12-HDDA molecule in the binary complex. Within the active site, the carboxyl group of dodecanoic acid forms the same interactions as those described earlier for the carboxyl group of 12-HDDA. The long hydrophobic chain of dodecanoic acid extends away from the carboxyl-binding site toward the catalytic zinc, with a path similar to that observed for the 12-HDDA molecule. The terminal methyl group of the inhibitor appears to approach the zinc site closely, leaving no apparent room for a water molecule between the end of the acyl chain and the active site zinc ion. The presence of a water molecule between the inhibitor and the active site zinc seems unlikely because the electron density was continuous from the carboxyl end up to 2.7 Å from the active site zinc and the inhibitor could account for all the observed electron density. Direct mass spectrometric analysis of the dodecanoic acid used for the crystallization work showed no contamination (data not shown). The hydrophobic contacts made by the acyl chain of the inhibitor are similar to those observed for 12-HDDA.

Interactions in the coenzyme binding site. In the coenzyme-binding site, only the residues projecting from the catalytic domain undergo a minor shift in their position upon formation of the inhibitor ternary complex. These side chain movements are a consequence of the small movement in the catalytic-domain in the ternary complex. In both the apoenzyme and the FDH·12-HDDA binary complex, a buffer phosphate ion occupies the pyrophosphate binding site, where it interacts with Arg368 and His45. His45 is a highly conserved residue among FDH isozymes and has three conformations in the structures reported here. All of these conformations result from rotation about the $C_\alpha-C_\beta$ bond and enable His45 to interact with the bound phosphate or the conenzyme in different ways. In the FDH·NAD^+· dodecanoic acid ternary complex, His45 has two conformations, suggesting that His45 can interact with the coenzyme, either through its adenosine phosphate moiety or through the 2′-hydroxyl of the nicotinamide ribose.

Zinc coordination state in FDH complexes. The ligand environment of the active site zinc shows distinct changes in the different FDH structures. We utilized the anomalous signal from zinc to experimentally phase our structures so that the positions of the active site zinc ions in these complexes could be directly assigned without the bias inherent in phases obtained through molecular replacement. In the apoenzyme, the active site zinc has four ligands, similar to other ADHs (Figure 4a) (*19*, *20*, *22*). This tetrahedral coordination environment has three ligands contributed by the enzyme (Cys44, His66, and Cys173), and a water molecule occupies the fourth coordination site. The highly conserved amino acid, Glu67, is 4.5 Å from the zinc in both the subunits of the apoenzyme (Figure 4a). The distance between Glu67 and the catalytic zinc is similar to that observed in all non-Class III ADH structures. This particular orientation of Glu67 is stabilized by hydrogen bonds between its carboxylate oxygens and the guanidine nitrogens of Arg368, similar to that observed in all other ADH structures.

The binding of 12-HDDA does not appear to influence the coordination environment of the active site zinc except by displacing the zinc bound water molecule when the hydroxyl group of 12-HDDA coordinates with zinc in the FDH·12-HDDA binary complex. In this complex, Glu67 is 4.7 Å from the active site zinc and interacts with the guanidium group of Arg368 and a water molecule, as in the apoenzyme.

The ligand environment of the active site zinc undergoes a more dramatic change upon formation of the FDH·NAD^+· dodecanoic acid ternary complex. The active site zinc is displaced 2.1 Å from its position in the apoenzyme and toward the back of the active site and Glu67 (Figure 4b,c). This movement of the catalytic zinc reorients its ligands, Cys44, His66, and Cys173 in order to accommodate the

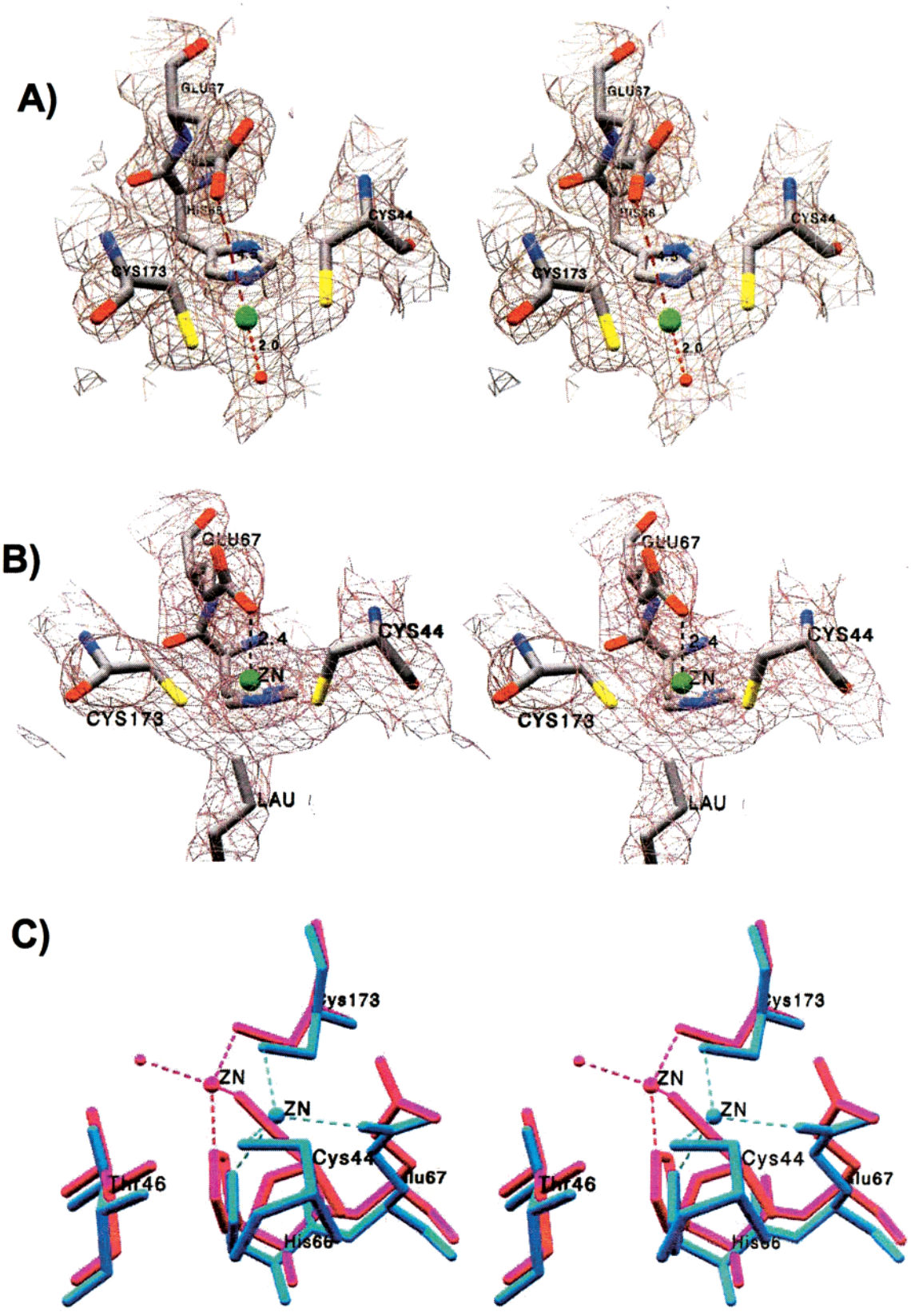

FIGURE 4: Coordination environment of the active site zinc in the apo form of FDH and FDH·NAD^+·dodecanoic acid ternary complex. (A) Electron density for the active site zinc and its ligands in the original MAD map contoured at one standard deviation for the apoenzyme. (B) Electron density for the active site zinc and its ligands and dodecanoic acid (LAU) in the original MAD map contoured at one standard deviation for the FDH·NAD^+·dodecanoic acid ternary complex. (C) The relative positions of the active site zinc and its ligands in the apoenzyme (red) and FDH·NAD^+·dodecanoic acid ternary complex (blue) are displayed. The coenzyme binding domains (residues 180−289 and 301−320) of the apoenzyme and the ternary complex were aligned before comparing the coordination environment of active site zinc in the apoenzyme and the FDH·NAD^+·dodecanoic acid ternary complex.

displacement (Figure 4c). Cys44 and Cys173 exhibit larger changes in conformation than does His66. Repositioning of the zinc and its ligands appears to transmit structural changes throughout the catalytic domain that cause the shift of other residues away from the coenzyme-binding domain by 0.4−1.5 Å, depending on their distance from the active site zinc. The observed shift can be described as a 0.7° rotation of the catalytic domain away from coenzyme-binding domain, leading to a slightly more open domain position. The inner coordination sphere of the catalytic zinc ion now includes the side chain of Glu67. As a consequence of these new interactions, Glu67 breaks its previous association with Arg368 and rotates to coordinate with the zinc (Figure 4c). The active site zinc retains tetrahedral coordination geometry, but now Cys44, His66, Glu67, and Cys173 are the four ligands. Glu67 is 2.4 Å from the active site zinc and the terminal methyl group of the dodecanoic acid is located ∼2.7 Å from the active site zinc.

DISCUSSION

The initial structural and kinetic studies on horse liver ADH (*18*, *19*, *23*, *24*) established the basis for interpreting the structure−function relationships within the alcohol dehydrogenase enzyme family and NAD^+-dependent oxidoreductases. All of the structurally studied mammalian alcohol dehydrogenases, except FDH, predominantly follow an ordered bi bi kinetic mechanism with primary alcohols where the coenzyme is the first substrate to bind and the last product to leave the enzyme during a catalytic cycle (*23*, *24*). In horse liver ADH, binding of the coenzyme induces the catalytic-domain to move by 10° toward the coenzyme-binding domain. This conformational change narrows the active site located in the cleft between the two domains and brings key active site residues into position for catalysis (*19*). The two domain positions observed in the apoenzyme and holoenzyme of horse ADH have been referred to as "open" and "closed". Among the alcohol dehydrogenase structures solved so far, the domain motion between the apo- and holoenzyme of horse liver alcohol dehydrogenase is the largest. Intermediate positions of the catalytic domain have been observed in binary and ternary complexes of class I cod liver and class II mouse liver alcohol dehydrogenases (*25*, *26*). However, the structures of the respective apoenzymes have not been reported. Hence, domain movement has been inferred to be present in all vertebrate ADHs by extrapolation to the horse EE isozyme. The intermediate catalytic-domain position in FDH:NAD(H) binary complex (*9*) and the random bi bi kinetic mechanism of FDH (*8*) suggested that the structural changes in FDH may not resemble those observed in horse liver ADH. Accordingly, the catalytic-domain conformation in the apo-FDH, FDH:12-HDDA binary, and FDH:NAD^+:dodecanoic acid ternary complexes were determined and compared with that of the FDH:NAD(H) binary complex. All comparisons were performed by aligning the "core" of the coenzyme-binding domains (residues 180−289 and 300−320) of the two forms being studied. As opposed to the dramatic domain movement observed in horse liver ADH, very little domain movement was observed between apo, binary, and inhibitor ternary complexes of FDH (Figure 1). The catalytic-domain position in these FDH complexes is about halfway between the fully open conformation and the fully closed form of horse liver ADH. Thus, for alcohol binding in FDH, there is a single partially open catalytic-domain position coupled with highly flexible loops near the mouth of the active site. The relatively stable domain conformation apparently keeps the key substrate-binding residues in the proper position for catalysis, while the mobile nature of the loops near the mouth of the active site provides the needed flexibility for binding the varied substrates utilized by FDH. This is consistent with the random addition of substrates exhibited by FDH and the ability of this enzyme to accept substrates as diverse as HMGSH and 12-HDDA.

The volume of the active site of FDH is substantially larger than that observed in horse ADH, which explains the preference of FDH for long-chain alcohols/aldehydes and glutathione adducts such as HMGSH and GSNO as substrates. The majority of the active site is comprised of hydrophobic residues that project from all sides. At the base of the substrate-binding site, a polar binding pocket is formed by the presence of Gln111, Arg114 ,and Lys283. Several studies have probed the importance of this positively charged pocket in the preferential binding of physiological substrates such as HMGSH. Site-directed mutagenesis studies of Arg114 suggest that it plays a critical role in the binding of both 12-HDDA and HMGSH (*21*). An ω-carboxylate group on a long chain alcohol increases the second-order rate constant by more than an order of magnitude over a similar alcohol lacking such a group (*6*, *27*). The orientation and interactions of 12-HDDA and dodecanoic acid in the FDH·12-HDDA and FDH·NAD^+·dodecanoic acid complexes are also consistent with these observations. In the FDH·12-HDDA binary complex, the strong and continuous electron density near the carboxyl end of 12-HDDA suggests that the anchoring point of the molecule in FDH active site is the carboxyl group.

Arg114 has two conformations in the three structures reported here (Figures 2 and 3). The conformation in which it bends away from the carboxyl group of the substrate (Figure 3) appears to predominate when the substrate is bound in the active site (like in the ternary complex). Thus, Arg114 could participate in the binding of 12-HDDA in two ways: (i) a direct role in substrate binding brought about by a small rotation of the side chain thereby placing the guanidium group appropriately for the hydrogen bonding interaction; or (ii) an indirect role in substrate binding by affecting the orientation of amide moiety of Gln111 conducive to hydrogen bonding interaction with the carboxyl group of the substrate. On the basis of the structural evidence, we suggest that the later is more likely, but we cannot rule out the former.

Medium-chain fatty acids, 8−10 carbons in length, activate the oxidation of short chain alcohols such as ethanol (*6*). A positively charged residue in the active site like Arg114 was proposed to be important in the binding of the anionic group of the activator (*21*, *27*). The mechanism by which fatty acids enhance the oxidation of short chain alcohols is evident from the FDH·NAD^+·dodecanoic acid ternary complex. The long-chain fatty acid binds to FDH through its carboxyl group and its long hydrophobic carbon chain interacts with apolar residues along the active site. The binding of slightly shorter fatty acyl chains would reduce the dimensions of the large FDH active site but leave room for the binding of short alcohols at the zinc. Consequently, short-chain alcohols gain sufficient productive interactions at the catalytic zinc.

A change in the coordination environment of active site zinc is observed in the different FDH structures reported here. The presence of Glu67 in the inner coordination of the active site zinc in the previously published FDH·NAD(H) binary complex suggested a unique zinc-coordination environment in FDH. By determining the structures of the apoenzyme, an enzyme:alcohol binary complex, and an inhibitor ternary complex, we gain a more complete understanding of the coordination environment of the catalytic zinc ion. These structures show that Glu67 coordinates with active site zinc only under certain conditions. Using molecular dynamic and quantum mechanical computations, Ryde proposed that Glu67 (Glu68 in horse liver ADH) could coordinate to the active site zinc intermittently during catalysis in horse liver ADH (*28*). However, the actual displacement of the active site zinc during these changes in coordination was an unexpected finding in FDH. It is also evident from the available FDH structures that the binding of coenzyme is associated with the zinc movement that brings Glu67 into its coordination sphere. Whether the movement of zinc is dependent on the oxidation state of the coenzyme is an important consideration. The likelihood of the coenzyme being NAD^+ in the FDH·NAD^+·dodecanoic acid complex is high because the crystals were obtained by initially soaking the apoenzyme crystals with the inhibitor dodecanoic acid followed by a second soak with a mixture of NAD^+ and dodecanoic acid. In other studies employing absorption spectra of the binary complexes of Co^{2+}-substituted FDH with NAD^+ and NADH, the binary complex spectra are very similar to each other but different from that of the apo form of the Co^{2+}-enzyme (*29*). This suggests that the electronic environment near the catalytically competent Co^{2+} metal ion is similar in both the NAD^+ and NADH complexes, supporting the idea that the zinc movement observed in our structures may be independent of the oxidation state of the coenzyme.

Displacement of the active site zinc toward Glu67 by the coenzyme and its interaction within the inner coordination sphere of the catalytic metal have several consequences. The interaction between the zinc and its bound water molecule clearly weakens with Glu67 coordination. This could facilitate displacement of the water molecule by an incoming substrate hydroxyl group. The discontinuous electron density of the hydroxyl end of 12-HDDA in our FDH·12-HDDA binary complex could be explained by the nearly equal competition for zinc coordination by two groups with similarly high pK_a values (pK_a > 14 for both water and alcohols). Thus, efficient exchange of ligands (i.e., release of the zinc-bound water molecule) could be promoted by a reduction in the electrophilic character of the catalytic zinc through transient coordination by Glu67. Optimal transfer of the hydride ion from the substrate molecule to the coenzyme requires that the hydroxyl group of the substrate be positioned in manner similar to that of 12-HDDA in our binary complex (Figure 2). Thus, if the ligand exchange step proceeds through a coordination environment like that observed in our dodecanoic acid ternary complex, it is likely that the zinc is pulled back to its original position by the substrate during the catalytic cycle. The development of the negatively charged alcoholate anion could drive Glu67 off the zinc ion and cause an inversion of the coordination geometry. The transition between these two coordination environments is likely to proceed through a transient pentacoordinated zinc intermediate with trigonal-bipyramidal geometry, where the solvent water molecule and Glu67 occupy axial positions.

It is possible that coordination of the active site zinc ion by Glu67 represents an intermediate step in the catalytic pathway of all ADH isozymes (*28*). FDH and other ADHs have a similar overall structure and catalyze the same reaction with different substrate specificities. Consequently, it would be expected that the catalytic steps are conserved between FDH and other ADH isozymes. In addition, FDH is likely to have formed the basis for the development of new activities within the ADH family as gene duplication and subsequent divergence of these paralogous genes gave rise to new functions. The coordination of the catalytic zinc to Glu67 would facilitate ligand exchange during catalysis and explain why Glu67 is highly conserved in all ADHs. The importance of the negative charge of Glu67 is evident from the decreased affinity for the substrate analogue trifluoroethanol, the decreased affinity for NAD^+, and the decreased turnover number exhibited by a Gln for Glu68 mutant form of Yeast ADH (*30*). Displacement of the active site zinc, in addition to catalytic-domain movement, could represent the mechanism by which the coenzyme aids in the binding of substrates and release of products in other ADH isozymes.

REFERENCES

1. Koivusalo, M., Baumann, M., and Uotila, L. (1989) *FEBS Lett. 257*, 105−109.
2. Jensen, D. E., Belka, G. K., and Du Bois, G. C. (1998) *Biochem. J. 331*, 659−668.
3. Liu, L., Hausladen, A., Zeng, M., Que, L., Heitman, J., and Stamler, J. S. (2001) *Nature 410*, 490−494.
4. Deltour, L., Foglio, M. H., and Duester, G. (1999) *J. Biol. Chem. 274*, 16796−16801.
5. Wagner, F. W., Pares, X., Holmquist, B., and Vallee, B. L. (1984) *Biochemistry 23*, 2193-2199.
6. Moulis, J. M., Holmquist, B., and Vallee, B. L. (1991) *Biochemistry 30*, 5743−5749.
7. Kaiser, R., Holmquist, B., Vallee, B. L., and Jornvall, H. (1989) *Biochemistry 28*, 8432−8438.
8. Sanghani, P. C., Stone, C. L., Ray, B. D., Pindel, E. V., Hurley, T. D., and Bosron, W. F. (2000) *Biochemistry 39*, 10720−10729.
9. Yang, Z. Y., Bosron, W. F., and Hurley, T. D. (1997) *J. Mol. Biol. 265*, 330−343.
10. Otwinowski, Z., and Minor, W. (1997) *Methods Enzymol. 276*, 307−326.
11. Terwilliger, T. C., and Brendzen, J. (1999) *Acta Crystallogr., Sect. D: Biol. Crystallogr. 55* (Part 4), 849−861.
12. Terwilliger, T. C. (2000) *Acta Crystallogr., Sect. D: Biol. Crystallogr. 56* (Part 8), 965−972.
13. Brunger, A. T., Adams, P. D., Clore, G. M., DeLano, W. L., Gros, P., Grosse-Kunstleve, R. W., Jiang, J. S., Kuszewski, J., Nilges, M., Pannu, N. S., Read, R. J., Rice, L. M., Simonson, T., and Warren, G. L. (1998) *Acta Crystallogr., Sect. D: Biol. Crystallogr. 54*, 905−921.
14. Meijers, R., Morris, R. J., Adolph, H. W., Merli, A., Lamzin, V. S., and Cedergren-Zeppezauer, E. S. (2001) *J. Biol. Chem. 276*, 9316−9321.
15. Al-karadaghi, S., Cedergren-Zeppezauer, E., Petrantos, K., Hovmoller, S., Terry, H., Dauter, Z., and Wilson, K. S. (1994) *Acta Crystallogr., Sect. D 50*, 793−807.
16. Jones, T. A., Zou, J. Y., and Kjeldgaard, M. (1991) *Acta Crystallogr., Sect. A 47*, 110−119.
17. Kleywegt, G. J., and Jones, T. A. (1997) *Methods Enzymol. 277*, 208−230.
18. Ramaswamy, S., Eklund, H., and Plapp, B. V. (1994) *Biochemistry 33*, 5230−5237.

19. Eklund, H., Plapp, B. V., Samama, J. P., and Branden, C. I. (1982) *J. Biol. Chem. 257*, 14349−14358.
20. Eklund, H., Nordstrom, B., Zeppezauer, E., Soderlund, G., Ohlsson, I., Boiwe, T., Soderberg, B. O., Tapia, O., Branden, C. I., and Akeson, A. (1976) *J. Mol. Biol. 102*, 27−59.
21. Engeland, K., Hoog, J. O., Holmquist, B., Estonius, M., Jornvall, H., and Vallee, B. L. (1993) *Proc. Natl. Acad. Sci. U.S.A. 90*, 2491−2494.
22. Hurley, T. D., Bosron, W. F., Stone, C. L., and Amzel, L. M. (1994) *J. Mol. Biol. 239*, 415−429.
23. Sekhar, V. C., and Plapp, B. V. (1990) *Biochemistry 29*, 4289−4295.
24. Sekhar, V. C., and Plapp, B. V. (1988) *Biochemistry 27*, 5082−5088.
25. Ramaswamy, S., El-Ahmad, M., Danielsson, O., Jornvall, H., and Eklund, H. (1996) *Protein Sci. 5*, 663−671.
26. Svensson, S., Hoog, J. O., Schneider, G., and Sandalova, T. (2000) *J. Mol. Biol. 302*, 441−453.
27. Holmquist, B., Moulis, J. M., Engeland, K., and Vallee, B. L. (1993) *Biochemistry 32*, 5139−5144.
28. Ryde, U. (1995) *Protein Sci. 4*, 1124−1132.
29. Maret, W. (1989) *Biochemistry 28*, 9944−9949.
30. Ganzhorn, A. J., and Plapp, B. V. (1988) *J. Biol. Chem. 263*, 5446−5454.
31. Guex, N., and Peitsch, M. C. (1997) *Electrophoresis 18*, 2714−2723.

BI0257639